Computer-Simulation Methods in the Study of Noncrystalline Materials

Fumiko Yonezawa

Computer-assisted physics can be considered the third approach besides experimental and theoretical physics. Numerical simulations are especially useful in the study of noncrystalline materials such as liquids, glasses, amorphous solids, and liquid crystals. Some applications of computer simulations to these materials are discussed.

In physics, as in any other field of natural science, research has been traditionally carried out through experiments and theoretical analyses. For the last few decades, however, a new trend of computer-assisted physics has been established mainly as a result of remarkable developments in computer technology. Today, the approach of computational physics is even mentioned as the third physics, following experimental and theoretical physics. This terminology by no means indicates that computer-assisted physics ranks third; it simply reflects the fact that this approach comes chronologically after the first two.

As a matter of fact, this new branch of research has made a number of impossibilities possible and brought about a series of breakthroughs in physics. Judging from the extremely rapid progress in the performance of computers and from the increasing need for the understanding of systems far more complex than the traditional techniques of natural science have ever handled, it is expected that the roles played by computer-assisted sciences will become important in the century to come.

In Japan the significance of computer-assisted physics was pointed out relatively early, and in fiscal year 1991, a new project, "Computational Physics as a New Frontier in Condensed Matter Research," started under the support of the Grant-in-Aid for Scientific Research on Priority Areas from the Ministry of Education, Science, and Culture of Japan (*1*). The project consists of four major subjects: (i) design of materials properties from first principle, (ii) strongly correlated quantum systems, (iii) cooperative phenomena in complex systems, and (iv) dynamics in many-body and macroscopic systems. My colleagues and I performed the work to be discussed in this article as a part of this project.

Among other things, the methods of computer simulations are a champion of computational physics. Roughly speaking, computer simulations consist of two steps: the first is the construction of a physical system according to some given rules, and the second is the measurement (or calculation) and analysis of various physical properties of that system. In the study of condensed matter, the first step requires the realization of a system composed of many particles that mutually interact by means of theoretically determined potentials. The time development of the physical system thus constructed is generally solved by either stochastic or deterministic procedures.

As for stochastic procedures, the Metropolis algorithm (*2*), which has been proven to lead a system to its thermal equilibrium, is widely accepted and forms the main part of the Monte Carlo simulations. On the other hand, deterministic procedures assume that particles obey classical mechanics so that coupled Newtonian equations describe what happens in condensed matter. This technique is referred to as molecular dynamics (MD) simulation (*3*, *4*). In this article, I present applications of MD simulation to the study of (i) relaxation and slow dynamics near glass transition, (ii) crystal-to-smectic transition in liquid crystals, and (iii) atomic and electronic configurations in amorphous Si:H.

Since the advent of high-speed computers, MD simulation has successfully contributed to a better understanding of nature by verifying unexpected facts and introducing new concepts, all of which never have been predicted previously by analytical theories. The occurrence of the liquid-to-crystal transition (the so-called Alder transition) in a system of only repulsive forces and the behavior of the long-time tails of the velocity autocorrelation function for a liquid are only a few examples.

The reason for this success is that computer simulations have much wider scope than conventional experimental and theoretical physics. The advantages of computer simulations over experimental physics are clearly manifested in the description of how they overcome the difficulties of experiments. (i) Computer simulations can deal with systems that do not exist in reality and are therefore experimentally inaccessible. For example, it is possible, for the sake of revealing fundamental rules of nature, to construct systems composed of particles interacting by means of imaginary model potentials. (ii) A wide variety of physical properties are measured in computer simulations, whereas only a limited class of physical properties can be observed in laboratories. For example, the full information about the positions and velocities of all particles in a simulation system is available, from which any desired microscopic physical quantities can be derived. (iii) Although some extreme limits cannot be realized even by state-of-the-art apparatus, they are produced in computers. Examples include exceedingly high pressures and extraordinarily rapid quench rates. (iv) Although it is difficult to establish experimentally unique relations between input and output data, the cause and effect between them can be clarified without any ambiguity in computer simulations because input conditions are controlled.

The methods of computer simulations can be compared with those of theoretical physics as follows: To make real physical systems tractable by theories, it is always necessary to extract essential aspects and construct simple models. Very often, rigorous solutions are achieved only for oversimplified models; accordingly, the physical relevance of the solutions is questionable. For less simple models, on the other hand, problems must be solved with the use of approximations, but the validity of these approximations is not necessarily guaranteed from a physical point of view. Computer simulations are free from these difficulties because exact solutions are obtained even for complex systems without approximations. As a result, it is possible to study models much closer to realistic materials. It must be noted, however, that computer simulations are carried out only for finite-size systems during a finite observation time. Techniques that minimize the effects of these limitations must be elaborated in the actual processes of simulations.

Relaxation and Slow Dynamics near Glass Transition

In the field of condensed-matter physics, the investigation of crystalline materials is more advanced than that of noncrystalline materials. It was as early as the 1910s when the x-ray diffraction technique for the analysis of crystalline structures was first proposed, and the atomic structures of crystals have been fully analyzed since then. After the establishment of quantum mechanics in

Department of Physics, Keio University, 3-14-1 Hiyoshi, Kohokuku, Yokohama 223, Japan.

the 1920s, the fundamental theories for the electronic properties of crystals were constructed essentially in the form of Bloch's theorem. In these experimental and theoretical investigations of crystals, full use has been made of periodicity (or in other words, translational symmetry).

There exists still another category of materials that includes noncrystalline solids and liquids in general. The atomic configurations of the materials in this category are noncrystalline, nonperiodic, liquid, disordered, random, amorphous, and glassy, all adjectives that are normally used synonymously. Experiments with these amorphous materials give only limited information about the atomic configurations, such as the absence of the long-range order, in that there remains no vestige of translational symmetry, and the existence of the short-range order, in that the local environment of each atom in a disordered structure is similar to that in a crystal.

Disordered systems are examples in which the methods of computer simulations, in particular MD techniques, fully prove their worth. As a matter of fact, since the introduction of the MD methods in the 1950s, the most widely studied subject has been liquids. With this situation in mind, we apply our MD programs to the study of amorphous materials.

We carried out constant-pressure MD of quenching to construct glasses composed of atoms that interact by means of the Lennard-Jones (LJ) potentials (*5*, *6*). The results can be closely compared with the experimental results when the constant-pressure technique is used because most experiments are performed under a constant (atmospheric) pressure. We used the periodic boundary condition, the number N of atoms was 864, and the time step for integration was 0.5×10^{-14} s for Ar. We realized Ar glasses by cooling an LJ liquid with quench rates as high as 10^{12} K s^{-1}. This quench rate is greater by a few orders of magnitude than the highest possible quench rates in laboratories. The limited capability in the production of high quench rates in laboratories has prohibited the glass formation of simple systems in which atoms interact through isotropic potentials. This is where the techniques of computer simulations are decisive because, in computers, the quench rates can be raised, in principle, as high as desired.

The atomic configurations of stable glasses thus obtained are characterized by the coexistence of large clusters composed of atoms with icosahedral symmetry and clusters of atoms with crystalline symmetry (Fig. 1). Atoms are classified into three categories: those with icosahedral symmetry, those with crystalline symmetry, and others. The classification is performed according to the local structures of atoms defined by the bond angles and positions relative to neighboring atoms.

Since the 19th century, it has been known that fivefold symmetry is incompatible with translational symmetry for a crystal. On the other hand, it was pointed out by Frank in 1952 that small particles can take shapes having fivefold (or more precisely, icosahedral) symmetry because the icosahedral structure gives the lowest local energy owing to the large coordination numbers (*7*). From the same energy argument, the local icosahedral configurations are expected to appear in disordered systems in which there exists no translational order. Our simulations lend support to the prediction by Frank and ascertain that large clusters, as represented by Fig. 1, stabilize glassy structures that are realized only through relatively slow quench rates.

The essential nature of amorphous structures is also studied by observation of the ways in which the structures relax to the stable states across activation barriers. To provide such disordered systems, we constructed by MD a supercooled LJ liquid and an LJ glass. To study the microscopic structures, we introduced the following microscopic parameters: (i) $v = V/N$, where V is the total volume, is the volume per atom, usually referred to as the atomic volume, which gives an idea about the spacial flexibility of each atom; (ii) δv, the root-mean-square volume of the Voronoi polyhedra, is the fluctuation parameter, which is a measure of fluctuations in the microscopic structure; (iii) $\langle \xi \rangle_i$ is the distortion parameter, which is related to the shapes of the atomic volumes and describes the local distortion; (iv) $\langle |\hat{\omega}_6| \rangle_i$ is the local symmetry parameter, which monitors whether an atom has the local structure of icosahedral or crystalline symmetry; and (v) n_α are the Voronoi face parameters, which give the degree of disorder or amorphousness around each atom.

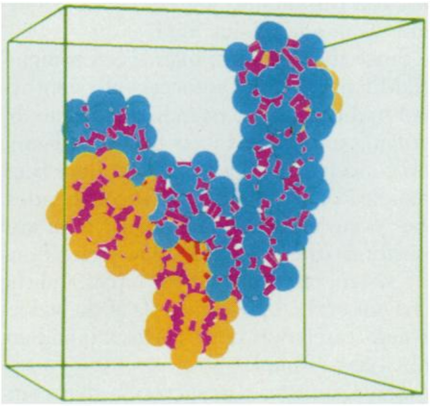

Fig. 1. Amorphous structures constructed by MD simulation exhibit clusters composed of atoms with local icosahedral symmetry (blue atoms) and crystalline symmetry (yellow atoms).

The time needed to relax a supercooled liquid to a crystalline structure (Fig. 2A) is one order of magnitude less than that to relax a glass to a crystal (Fig. 2B). From a careful analysis of these results, we can see that relaxation from disordered structures, liquid and glass, to a crystalline state takes place in three stages: local rearrangement, more extensive rearrangement, and finally, drastic rearrangement of atomic configurations. In the case of annealing a supercooled liquid, there is enough room for the large fluctuations to occur so that the transition from the second to third stage is manifested by the noticeable increase in δv (Fig. 2A). This situation is not observed in the case of annealing a glass (Fig. 2B) because the packing of atoms is too tight. This kind of microscopic analysis is impossible by experiments.

In a fluid more complex than the simple LJ liquid, the relaxation of atoms in the deeply supercooled region is much slower, and crystallization does not occur during observation time. It is empirically known that relaxation functions in this region are well described by stretched-exponential functions. For investigation of this problem of slow dynamics in supercooled liquids by means of MD simulation, binary mixtures of soft spheres (*8*, *9*) and LJ atoms (*10*) were chosen as model systems.

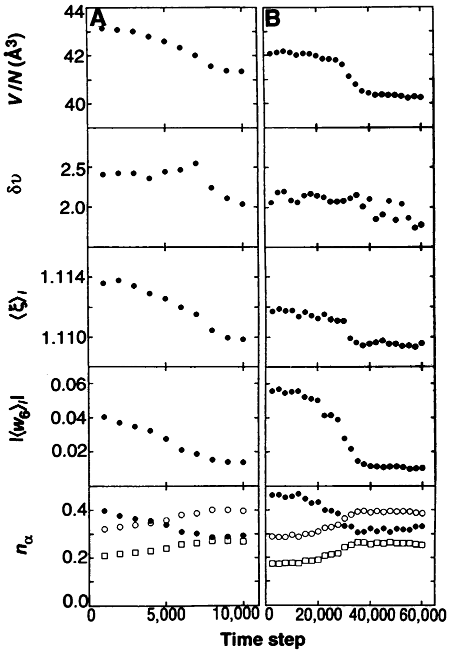

Fig. 2. Microscopic structure parameters versus annealing time at (**A**) normalized temperature $T^* = 1.08$, where a supercooled liquid relaxes to a crystal, and (**B**) $T^* = 0.80$, where a glass relaxes to a crystal. Symbols for n_α: (□) $\alpha = 4$; (●) $\alpha = 5$; and (○) $\alpha = 6$.

At a relatively high temperature (T = 60 K), the number-density autocorrelation function decays continuously to zero after 0.1 ns (Fig. 3) (*10*). On the other hand, at a deeply supercooled temperature (T = 45 K), there appear to be three stages in relaxation. In the first stage ($t < 10^{-3}$ ns), there is an appreciable drop of $F(\mathbf{k}_{\text{peak}}, t)$, the dynamical structure factor defined by the density correlation function, where $\mathbf{k}_{\text{peak}}$ is the wave vector at which the static structure factor $F(\mathbf{k}, 0)$ has a peak. In the second stage (10^{-3} ns $< t <$ 0.1 ns), $F(\mathbf{k}_{\text{peak}}, t)$ stays almost constant, and for the third stage, $F(\mathbf{k}_{\text{peak}}, t)$ starts to decrease. Even after 1 ns, $F(\mathbf{k}_{\text{peak}}, t)$ is still larger than two-thirds of the value at the initial stage. The change in the behavior of $F(\mathbf{k}_{\text{peak}}, t)$ seems to occur between T = 50 and 49 K. This change is generally identified as the kinetic glass transition because the kinetic nature of the system is expected to change around this temperature T_x(50 K $> T >$ 49 K in this case), as suggested in Fig. 3.

To clarify the microscopic structure more closely, we found (*10*) the probabilities $P(r,t)$ of finding a particle at a distance r from the original position of that atom at time t = 0 (Fig. 4). At 55 K ($>T_x$), the time evolution of $P(r,t)$ demonstrates the shapes of simple diffusion, whereas at T = 46 K ($<T_x$), the first and second peak stay distinguished even after 2 ns. This time scale is much longer than that characteristic of atomic vibrations, which indicates that the atoms are captured in local minima.

Crystal-to-Smectic Transition in Liquid Crystals

Liquid crystals are the intermediate states of aggregation of organic compounds between crystalline solid and isotropic liquid. They are characterized by different degrees of molecular orientational order and a certain degree of fluidity. Altogether, up to 17 different thermotropic liquid-crystal phases have been identified. Here, we study smectic liquid-crystal phases in which molecules segregate into periodic layers, or, in other words, the time average of the molecular positions form a one-dimensional density wave. Various kinds of smectic modifications, namely, smectic A to K (*11*), have so far been found. We can roughly classify this rich variety of smectic phases into tilted and untilted structures, depending on whether the molecules on average are tilted or untilted against the layers. The two well-known untilted smectic phases are smectic A and B, where A has liquidlike layers and B has three-dimensional (3D) sixfold bond-orientational order (BOO).

We performed constant-pressure MD simulations of model systems composed of spherocylinders with (i) repulsive forces described by an inverse-power pair potential (*12*) and (ii) the LJ pair potential (*13*). It must be emphasized that in computer simulations, it is possible to treat repulsive and attractive forces separately and to clarify the role of each force. In both models, the anisotropy of the molecule was chosen to be 2, and the number N of molecules was 600. We started from a crystalline phase at low temperature and heated the system.

The specific volume V/N as a function of normalized temperature $T^* = T/T_g$, where T_g is the temperature of the glass transition, for model (i), characterized by repulsive forces alone (Fig. 5A), shows transition, a sharp change in volume at T^* = 1. To study the microscopic situation around the transition, we evaluated the anisotropy of the specific volume v_m associated with each molecule. We defined the specific volume v_m such that $v_m \equiv V/N = l_\parallel l_\perp^2$, where $l_\parallel = L_z/n_z$, n_z is the number of layers, $l_\perp = (L_\perp/n_\perp)^{1/2}$, and $n_\perp = N/n_z$. The ratio $l_\parallel/l_\perp$ is a measure of the anisotropy of the specific volume or of the space required for each molecule. For both models (i) and (ii), in the region we study, the anisotropy of the specific volume $l_\parallel/l_\perp$ is larger than the anisotropy of the molecule (Fig. 5B). There is

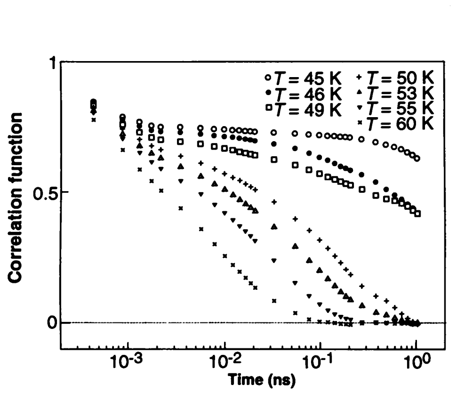

Fig. 3. The number-density autocorrelation function $F(\mathbf{k}_{\text{peak}}, t)$ versus time for seven different temperatures in the supercooled region of Ar.

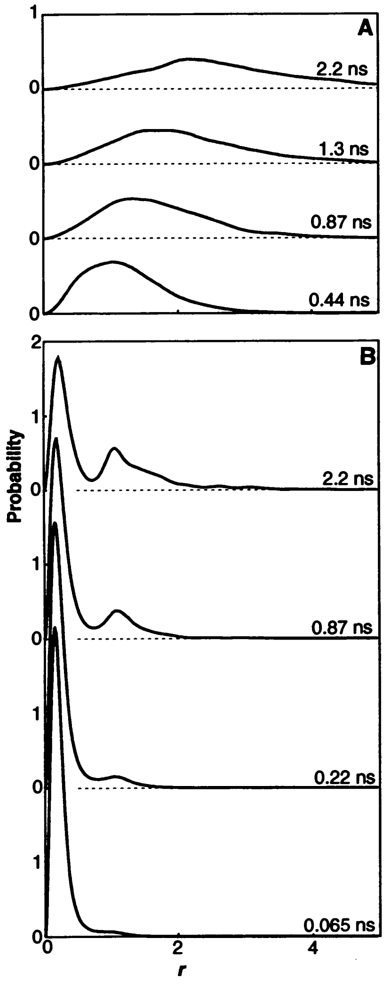

Fig. 4. The probability $P(r,t)$ for Ar of finding a particle at a distance $r = |\mathbf{r}|$ at time t (indicated in figure) and at (**A**) T = 55 K and (**B**) T = 46 K. The position $\mathbf{r}$ is measured from the original position of that atom at time t = 0.

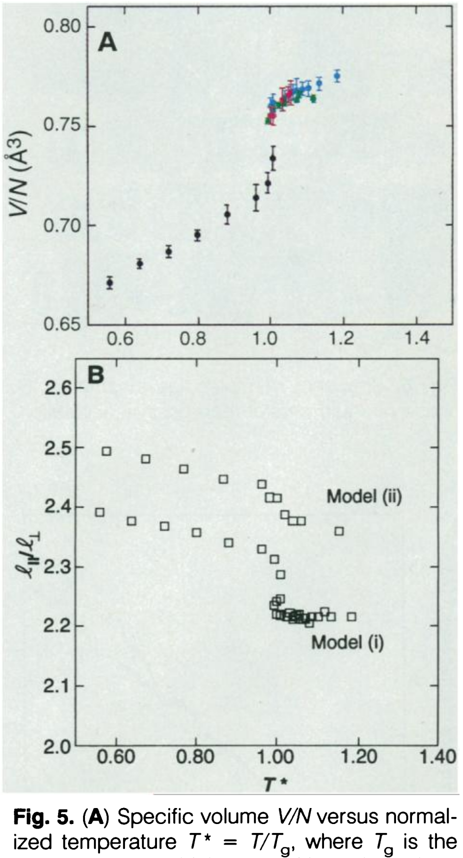

Fig. 5. (**A**) Specific volume V/N versus normalized temperature $T^* = T/T_g$, where T_g is the temperature at which a transition takes place from crystal (black) to smectic B phase of liquid crystal (red, blue, and green, representing results from different simulation methods). (**B**) Ratio of molecular lengths, $l_\parallel/l_\perp$, versus normalized temperature T^* for model (i) (potential with repulsive forces alone) and model (ii) (with both repulsive and attractive forces).

a discontinuous change in $l_\parallel/l_\perp$ in the transition-temperature region. In addition, $l_\parallel/l_\perp$ is larger for model (ii) because it includes an attractive part in the pair potential, and therefore, molecules within each layer become more condensed.

A snapshot of the system in the high-temperature phase clearly shows layer structure (Fig. 6). Analysis of the pair-distribution function shows that molecules in each layer take on disordered configurations. Besides, the liquidlike diffusion in each layer has been shown to exist with study of the mean-square displacement (MSD).

The MSD in the high-temperature phase for model (i) (Fig. 7) in directions perpendicular to the molecular axis (x and y axes) continues to increase, whereas the MSD in the direction along the molecular axis (z axis) becomes almost constant. From this behavior, we can see that diffusion takes place within layers, which is characteristic of the smectic liquid-crystal phase.

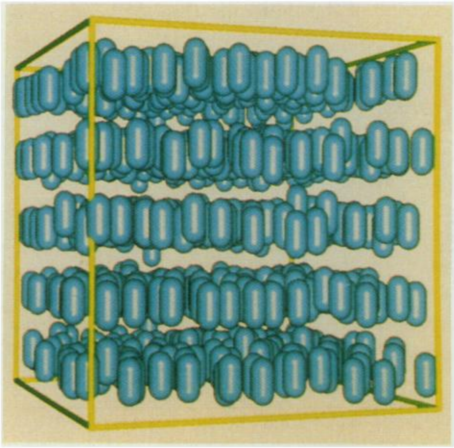

Fig. 6. Snapshot of molecules in smectic B phase of liquid crystal realized in a simulation box.

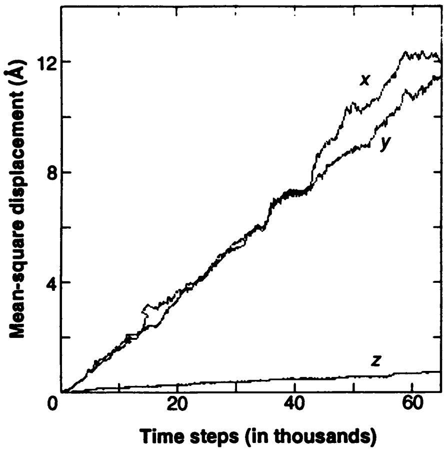

Fig. 7. Mean-square displacement in direction parallel (z axis) and perpendicular (x and y axes) to the molecular axis at $T^* = 1.02$.

To investigate the high-temperature phase in more detail, we examined the order parameter defined by

$$\Psi_6(\mathbf{r}_i) = \frac{1}{N_{\mathrm{nb}}} \sum_{j=1}^{N_{\mathrm{nb}}} \exp[i6\theta(\mathbf{r}_{ij})] \qquad (1)$$

where $\theta(\mathbf{r}_{ij})$ is the angle between a reference axis and the physical bond $\mathbf{r}_{ij}$ connecting neighboring molecules i and j. The sum is taken over all neighbors j of molecule i, where the number of neighbors is denoted by N_{nb}. These bond angles are measured by projection of the nearest neighbor molecules into the xy-plane, which is perpendicular to the molecular axis. We calculated the sixfold BOO parameter $C_6 = \mathrm{Re}[\langle\Psi_6(\mathbf{r}_{ij})\rangle]$ of each layer as a function of T^* (Fig. 8). Here, the bracket notation describes the average over all molecules i in a layer. In the crystalline phase, C_6 decreases as temperature increases, shows a jump at the crystal-smectic transition temperature ($T^* = 1$), and stays at an almost constant value of $C_6 \simeq 0.64$ in the smectic phase. This value is in good agreement with the values obtained from the electron diffraction (*14*) of a smectic B-phase material, which ranges roughly from 0.4 to 0.8. From this result, the existence of 3D BOO is clearly ascertained, and we can conclude that smectic B phase can appear even when the attractive part is absent in the intermolecular potential.

In this connection, the theory of 2D melting developed by Halperin and Nelson (*15*) predicts, between solid and liquid, an intermediate phase, named a hexatic phase, that exhibits short-range positional correlations and sixfold quasi–long-range BOO. Later, the possibility was suggested (*16*) of a liquid-crystal phase that consists of stacked 2D hexatic layers interacting to produce a 3D BOO. From the experimental side, liquid-crystal B phase was observed by x-ray studies (*17*). The occurrence of liquid-hexatic phase transition has been reported in a liquid-crystal free-standing film composed of a few layers (*18*).

With this situation in mind, we investigated the distribution of bond angles. The number of bonds divided by the system size clearly shows a periodicity of 60° (Fig. 9), which ascertains the existence of 2D hexatic layers. A remarkable point is that the curves for different layers almost coincide even after 5×10^4 time steps, suggesting that the 3D BOO is achieved owing to interacting 2D hexatic layers.

Atomic and Electronic Configurations in a-Si:H

Today, amorphous Si:H (a-Si:H) is one of the most promising materials for solar cells. Before 1975, however, the photovoltaic efficiency of a-Si was so low that the application to solar cells was practically out of the question. The low efficiency was entirely attributable to the dangling bonds that are abundant in a-Si.

In 1975, a-Si solar cells became realistic when the preparation technique of plasma decomposition of SiH_4 was introduced (*19*). Because a number of H atoms are present in this process, they are included in the Si network and are attached to almost all dangling bonds, thus preventing the generation of gap states. Since then, the photovoltaic efficiency of a-Si:H has been improved remarkably. In 1977, Staebler and Wronski found (*20*) that after a sample of a-Si:H prepared from SiH_4 by plasma decomposition is exposed to intense light, both photo and dark conductivity decrease by a few orders of magnitude, whereas the number of defects (mostly dangling bonds) increases. The created dangling bonds degrade the photovoltaic efficiency very seriously, and H seems to be the cause. It is therefore important and rather urgent to clarify, beyond predictions, the microscopic mechanism of this so-called SW effect (*21, 22*).

We studied the fundamental processes of the SW effect by ab initio MD simulation

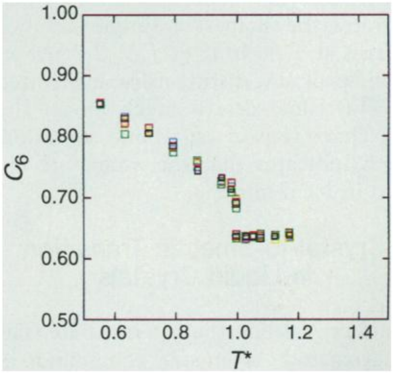

Fig. 8. The sixfold BOO parameter C_6 versus T^* (different colors describe the values for different layers).

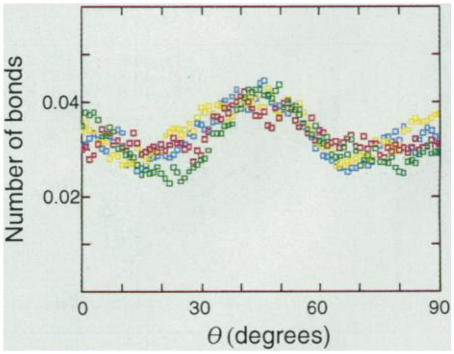

Fig. 9. Number of bonds versus angle between bonds measured in the x-direction of the simulation box. Different colors describe the values for different layers. Average taken over 1000 time steps before time step 5.0×10^4.

(*23, 24*). In this method, atoms and electrons are treated on the same basis, which is particularly appropriate for amorphous covalent systems because, in these systems, the distribution of atoms dominates the electron density at each point, thus defining the field in which an atom moves, which in turn determines the distribution of atoms. An efficient way to avoid the diagonalization was proposed by Car and Parrinello (*25*) and applied to various problems (*26–29*). This is the method we use.

Because the fundamental processes of the SW effect are regarded as local events, independent of the whole structure, we produced atomic and electronic configurations whose local environments simulated the configurations realized in a-Si:H. We did this by either the introduction of disorder in ordered structures or the construction of amorphous structures by quenching. In practice, we first confirmed that weak Si–Si bonds did exist in an amorphous network and then showed what would happen if there existed a H atom in the vicinity of such a bond. In our simulations, the time step for integration was 1.7×10^{-16} s, the number of atoms in a simulation cell was 8 or 64, and the maximum energy for the plane waves was 13.5 Ry. We used the density-functional method of Kohn and Sham (*30*) and the norm-conserving pseudopotential of Bachelet, Hamann, and Schlüter (*31*).

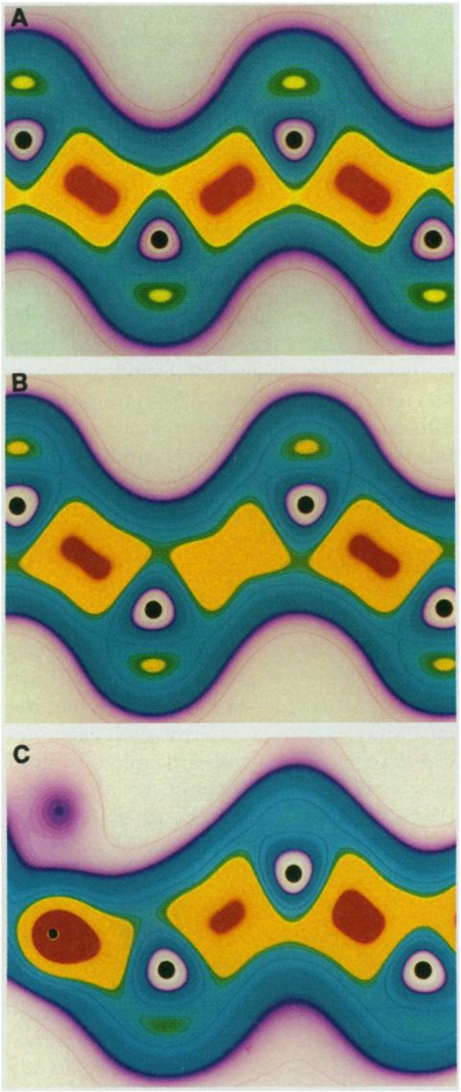

Fig. 10. Contour of the electron density along a network of bonds. (**A**) Crystalline Si, (**B**) a-Si, which includes a weak Si–Si bond, and (**C**) a-Si:H. Black circles denote Si atom and a small black circle denotes H atom. The density of electrons is highest in the red region and decreases in order of red, orange, yellow, green, blue, and white.

We first quenched liquid into amorphous solid. Because the estimated quench rates are as high as 10^{10} K s^{-1} in the process of plasma decomposition, techniques used in the preparation of a-Si:H, the quench rates 10^{10} to 10^{11} K s^{-1} in our computer simulations are comparable with those in the laboratory.

The obtained structure contains weak Si–Si bonds mainly because of geometrical requirements. The situation can be seen more clearly in the contours of the electron density (Fig. 10). We can see from Fig. 10B that when we say a bond is weak, we mean that the bond is longer as well as that the density of electrons is lower in the bonding orbital. For reference, we studied an excited state that simulates the situation in which electrons are excited by illumination by light. The results indicated that the length of a weak Si–Si bond is increased. In other words, weak bonds are weakened further as a result of light illumination. A Si–Si bond adjacent to a Si–H bond is also weakened, as demonstrated by the contour along the H–Si–Si–Si bonds in Fig. 10C. The electron density around the H atom is high because its electronegativity is higher, and accordingly, the Si–Si bond adjacent to Si–H bond becomes weak as a result of electron transfer to H.

As for the behavior of a H atom located in the neighborhood of a weak Si–Si bond, we found, from the calculation of the total energy, that, when the distance between two Si atoms in the weak Si–Si bond under consideration is not very long, there exists an off-bond metastable site for H, from which H diffuses out or to which H diffuses in relatively easily. When the distance between two Si atoms in the weak Si–Si bond is relatively long, a pair of Si–H and Si– (dangling) bonds are created. This microscopic configuration is relatively stable at room temperature, whereas H diffuses away when the temperature is higher.

In Fig. 11A, the contour is given for the off-bond metastable configuration. The electrons are shared not only by the two Si atoms under consideration but also by the Si atom in the nearest-neighbor position. The portion including an off-bond metastable site for H is presented in Fig. 11B. On the basis of these results, we propose a model for the fundamental mechanism of the SW effect in which the light-induced defect formation proceeds along off-bond metastable sites for H. Our model suggests that the degradation of the photovoltaic efficiency is decreased either by minimization of the distortions in the microscopic atomic structures or by substitution of H by some heavier elements, such as F.

Conclusion

The scope of computer simulations is not limited to numerical or quantitative achievement; rather, it is in qualitative aspects that the methods of computer-assisted physics reveal their greater power. Partly because of their high ability and partly because of the rapid progress in computers, the importance of these methods will increase in the future. However, it must always be borne in mind that physics is most essential in the performance of computer-assisted physics, just as in the case of experimental and theoretical physics.

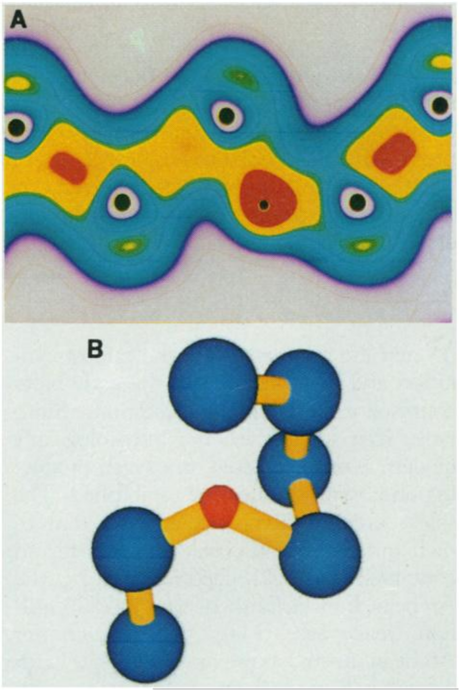

Fig. 11. (**A**) Contour of the electrodensity along the bonds of Si–Si–H–Si–Si–Si in the network of atoms, where H is at the site 0.4 off an Si–Si bond. (**B**) Network of Si–Si–H–Si–Si–Si–Si cut out from an amorphous configuration obtained by a quenching simulation from a liquid. Blue spheres denote Si atoms and red sphere denotes H atom.

REFERENCES AND NOTES

1. H. Takayama, *News Letter No. 1* (Research Group on a new project, "Computational Physics as a New Frontier in Condensed Matter Research" under the support of the Grant-in-Aid for Scientific Research on Priority Areas from the Ministry of Education, Science, and Culture of Japan, Tokyo, 1991).
2. N. Metropolis, A. Rosenbluth, M. Rosenbluth, A. Teller, E. Teller, *J. Chem. Phys.* **21** 1087 (1953).
3. F. Yonezawa, Ed., *Molecular Dynamics Simulations*, vol. 103 of the *Springer Series in Solid State Sciences* (Springer-Verlag, Heidelberg, 1992).
4. S. Nosé, Ed., *Prog. Theor. Phys. Suppl.* **103**, 1 (1991).
5. F. Yonezawa, in *Solid State Physics*, H. Ehrenreich and D. Turnbull, Eds. (Academic Press, New York, 1990), vol. 45, p. 179.
6. ______, S. Nosé, S. Sakamoto, *Neue Folge* **156**, 77 (1988).
7. F. C. Frank, *Proc. R. Soc. London Ser. A* **215**, 43 (1952).
8. J.-L. Barrat, J.-N. Roux, J.-P. Hansen, *Chem. Phys.* **149**, 198 (1990); J.-L. Barrat and M. L. Klein, *Annu. Rev. Phys. Chem.* **42**, 23 (1991).
9. Y. Hiwatari, in *Molecular Dynamics Simulations*, F. Yonezawa, Ed., vol. 113 of *Springer Series in Solid State Sciences* (Springer-Verlag, Heidelberg, 1992), p. 32.
10. S. Fujiwara and F. Yonezawa, in preparation.
11. S. Chandrasekhar, *Contemp. Phys.* **29**, 527 (1988).
12. K. M. Aoki and F. Yonezawa, *Phys. Rev. A* **46**, 6541 (1992).
13. K. Omata, K. M. Aoki, F. Yonezawa, in preparation.
14. M. Cheng, J. T. Hsi, R. Pindak, *Phys. Rev. Lett.* **61**, 550 (1988).
15. B. I. Halperin and D. R. Nelson, *ibid.* **41**, 121 (1978).
16. R. J. Birgeneau and J. D. Lister, *J. Phys. Paris* **39**, L399 (1978).
17. R. Pindak, D. E. Moncton, S. C. Davey, J. S. Goodby, *Phys. Rev. Lett.* **46**, 1135 (1981).
18. R. Geer *et al.*, *Nature* **355**, 152 (1992).
19. W. E. Spear and P. G. LeComber, *Solid State Commun.* **17**, 1193 (1975).
20. D. L. Staebler and C. R. Wronski, *Appl. Phys. Lett.* **31**, 292 (1977).
21. K. Morigaki, *Jpn. J. Appl. Phys.* **27**, 163 (1988).
22. W. B. Jackson and J. Kakalios, in *Amorphous Silicon and Related Materials*, H. Fritzsche, Ed. (World Scientific, Singapore, 1988), vol. 1, p. 247.
23. F. Yonezawa, S. Sakamoto, M. Hori, *J. Non-Cryst. Solids* **137**, 135 (1991).
24. F. Yonezawa and S. Sakamoto, *Optoelectronics-Devices Technol.* **7**, 117 (1992).
25. R. Car and M. Parrinello, *Phys. Rev. Lett.* **55**, 2471 (1985).
26. ______, *ibid.* **60**, 204 (1988); G. Galli, R. M. Martin, R. Car, M. Parrinello, *ibid.* **62**, 555 (1989); *ibid.* **63**, 988 (1989); I. Stich, R. Car, M. Parrinello, *ibid.*, p. 2243; G. Seifert, G. Pastore, R. Car, *J. Phys. Condens. Matter* **4**, L179 (1992); P. Ballone, W. Andreoni, R. Car, M. Parrinello, *Phys. Rev. Lett.* **60**, 271 (1988).
27. T. Oguchi and T. Sasaki, *Prog. Theor. Phys. Suppl.* **103**, 93 (1991).
28. Y. Morikawa, K. Kobayashi, K. Terakura, S. Blugerl, *Phys. Rev. B* **44**, 3459 (1991).
29. M. Tsukada, K. Kobayashi, N. Isshiki, H. Kageshima, *Surf. Sci. Rep.* **13**, 265 (1991).
30. W. Kohn and L. J. Sham, *Phys. Rev.* **140**, 1133 (1965).
31. G. B. Bachelet, D. R. Hamann, M. Schlüter, *Phys. Rev. B* **26**, 4199 (1982).
32. I thank my students S. Sakamoto, K. M. Aoki, S. Fujiwara, and K. Omata for collaboration.

RESEARCH ARTICLE

Microfossils of the Early Archean Apex Chert: New Evidence of the Antiquity of Life

J. William Schopf

Eleven taxa (including eight heretofore undescribed species) of cellularly preserved filamentous microbes, among the oldest fossils known, have been discovered in a bedded chert unit of the Early Archean Apex Basalt of northwestern Western Australia. This prokaryotic assemblage establishes that trichomic cyanobacterium-like microorganisms were extant and morphologically diverse at least as early as $\sim$3465 million years ago and suggests that oxygen-producing photoautotrophy may have already evolved by this early stage in biotic history.

When life originated and the rate of evolution and diversification of the early biota continue to be fascinating questions. Similarly, it is unclear when a physiologically modern ecosystem based on oxygen-producing photosynthesis became established. The sole source of direct evidence relevant to such questions is the paleobiologic record contained in rocks deposited during the Archean Eon of Earth history [$>$2500 million years ago (Ma)]. The search for Archean fossils, however, is fraught with difficulty: Few Archean sedimentary rocks have survived to the present, and paleobiologic evidence in most such units has been severely altered by metamorphism (*1*). The most promising terrain for such studies is that of the Pilbara Block of northwestern Western Australia, a region underlain by a 30-km-thick sequence of relatively well-preserved sedimentary and volcanic rocks that are $\sim$3000 to $\sim$3500 million years old (Fig. 1). From this region, I describe a diverse assemblage of filamentous microbial fossils detected in the Early Archean ($\sim$3465 million years old) Apex chert, cellular prokaryotes more than 1300 million years older than any comparable suite of fossils previously reported from the geologic record. Microfossils were first discovered in this deposit in 1986 (*2*); in a preliminary account, three taxa were identified (*3*). The eight additional species described here demonstrate that the Early Archean biota was more diverse than previously known (*3*, *4*), provide new understanding of the evolutionary status of early evolving microorganisms, and suggest that cyanobacterial oxygen-producing photosynthesizers may have already been extant this early in Earth history.

The Archean fossil record. Unlike that of the later Precambrian Proterozoic (*5*), the fossil record of the Archean is minuscule; few fossils have been detected and their study has been plagued by misinterpretation and questionable results (*4*). In order to establish the authenticity of Archean microfossils, five principal criteria must be satisfied (*3*). The putative microfossils must (i) occur in rocks of known provenance and (ii) established Archean age; (iii) be demonstrably indigenous to and (iv) syngenetic with the primary deposition of the enclosing rock; and (v) be of assured biological origin. All but a few of the microfossil-like objects reported from Archean sediments have failed to meet one or more of these requirements (*3*, *4*). Among recent such examples was the discovery of authentic microfossils in rocks evidently belonging to the Early Archean Warrawoona Group of Australia (*6*), a report unconfirmed because it has not proved possible to relocate the geologic source of the fossiliferous samples (*3*). Similarly, because of their simple morphology, solitary unicell-like spheroids reported from several Archean units (*7*, *8*) are best considered to be possibly rather than assuredly biogenic (*3*, *4*). Other than the filamentous Apex fossils discussed below, the relatively well-established Archean microfossil record consists of two types of cyanobacterium-like filaments from the $\sim$2750-million-year-old Tumbiana Formation of Western Australia (*4*); sheath-enclosed colonial unicells occurring in $\sim$3465-million-year-old sedimentary rocks of the Towers Formation, also of Western Australia (*2*); and narrow

---

The author is in the Center for the Study of Evolution and the Origin of Life, Institute of Geophysics and Planetary Physics, the Department of Earth and Space Sciences, and the Molecular Biology Institute, University of California, Los Angeles, CA 90024.